

Proton and Neutron Momentum Distributions in $A = 3$

Asymmetric Nuclei

A Hall A Collaboration Experiment

Proposal PR12-13-012 to Jefferson Lab PAC 42, July 2014

C. Hyde, S.E. Kuhn and L.B. Weinstein (co-spokesperson)
Old Dominion University, Norfolk VA

M. Braverman, E. Cohen, O. Hen (co-spokesperson),
I. Korover, J. Lichtenstadt, E. Piasetzky, and I. Yaron
Tel-Aviv University, Tel Aviv, Israel

W. Boeglin (co-spokesperson), P. Markowitz and M. Sargsian
Florida International University, Miami, FL

W. Bertozzi, S. Gilad (co-spokesperson), and V. Sulkosky
Massachusetts Institute of Technology, Cambridge, MA

D.W. Higinbotham, C. Keppel, P. Solvignon and S.A. Wood
Thomas Jefferson National Accelerator Facility, Newport News, VA

Guy Ron
Hebrew University, Jerusalem, Israel

R. Gilman
Rutgers University, New Brunswick, NJ

J.W. Watson
Kent State University, Kent, OH

A. Beck and S. Maytal-Beck
Nuclear Research Center Negev, Beer-Sheva, Israel

J. Beričič, M. Mihovilović, S. Širca, and S. Štajner
Jožef Stefan Institute, Ljubljana, Slovenia

D. Keller
University of Virginia, Charlottesville, VA

Vincenzo Bellini, Maria Concetta Suter and Francesco Mammoliti
INFN/CT and University of Catania, Catania, Italy

J. Annand, D. Hamilton, and D. Ireland
University of Glasgow, Glasgow, United Kingdom

A. Sarty
St. Mary's University, Halifax, Nova Scotia, Canada

L. Kaptari
Bogoliubov Lab. Theor. Phys., 141980, JINR, Dubna, Russia

C. Ciofi degli Atti
INFN Perugia, Perugia, Italy

(Dated: October 17, 2014)

In *non-interacting* Fermi systems with imbalanced number of two different Fermions, the average momentum per fermion is higher for the majority. Adding a strong short-range interaction between different fermions may invert the momentum sharing of the two components, making the minority move faster on average than the majority. This feature is due to the high momentum distribution being dominated by short distance pairs of different type Fermions. It is a common behavior that applies to systems ranging from ultra-cold atoms at neV energies to nucleons with MeV energies. In nuclei the nucleon-nucleon tensor force makes the neutron-proton short range correlated pair (*np*-SRC) the dominant component contributing to the high momentum of nucleons. In light neutron-rich nuclei such as ^3He , the average momentum of a proton should be higher than that of a neutron. In ^3He the average momentum of the neutron should exceed that of the protons.

We propose to verify the above prediction by measuring both the majority and minority nucleon momentum distributions of asymmetric $A = 3$ nuclei. We will do this by measuring the quasielastic $^3\text{H}(e, e'p)$ and $^3\text{He}(e, e'p)$ reactions at $Q^2 \approx 2 \text{ (GeV/c)}^2$ and $x_B = 1.2$ for missing momenta up to 450 MeV/c using the MARATHON target and the two HRS spectrometers in Hall A in kinematics which minimize the effects of Final State Interactions. Because the MARATHON target is limited to low luminosity, dead times and other rate effects will be negligible.

We plan to measure (a) the proton momentum distributions of both ^3He and ^3H in order to constrain detailed calculations of the $A = 3$ system, (b) the ratio of $^3\text{He}(e, e'p)/^3\text{H}(e, e'p)$ cross sections where the residual FSI will mostly cancel, and (c) the average kinetic energy of protons in the two nuclei as a function of the maximum measured momentum. It is crucial to measure these in $A = 3$ nuclei since these are the simplest asymmetric mirror nuclei and the only ones for which precisions calculations of the $(e, e'p)$ reaction exist.

This proposal was deferred by PAC 40. In this resubmission, we have reduced the requested beam time from 30 to 10 days by focussing on ^3He and ^3H , omitting the deuterium target and by reducing the beam time at large missing momentum. Because the MARATHON target is scheduled to be installed in Fall 2015, this is the last opportunity to approve any experiment to measure $^3\text{H}(e, e'p)$ at JLab.

We request 1 day of beam time for calibration and 9 days for the measurements of the $^3\text{H}(e, e'p)$ and $^3\text{He}(e, e'p)$ reactions. This will be the first $(e, e'p)$ measurement of ^3H and the only one on ^3He in reduced-FSI kinematics.

I. INTRODUCTION AND MOTIVATION

A. Common features of balanced (symmetric) and imbalanced (asymmetric) interacting two component Fermi systems

Many-body systems of two types of interacting fermions play an important role in nuclear, astro, atomic, and solid-state physics. Particularly intriguing are systems that include a short-range interaction that is strong between different fermions and weak between fermions of the same type.

Recent theoretical advances show that even though the underlying interaction between the fermions can be very different, these systems present several common features [1–4]. These features include the existence of a high-momentum tail ($k > k_F$, where k is the fermion momentum and k_F the Fermi momentum) that scales as C/k^4 and is dominated by short-range correlated (SRC) pairs of different fermions. The SRC pairs have large relative momentum between the fermions and small center-of-mass (CM) momentum, where large and small is relative to the Fermi momentum of the system. The scale factor, C , is known as Tan’s contact and fully controls the thermodynamics of the system [4].

The application to the nuclear case is more complicated because the range of the nuclear short-range tensor interaction is not much much smaller than the inter-nucleon separation and because it is a tensor interaction. This leads to a momentum density $n(k)$ at high momentum ($k > 1.5k_F$) proportional to V^2/k^4 where V is the momentum-dependent strength of the tensor interaction.

However, recent experimental studies of balanced (symmetric) interacting Fermi systems, with an equal number of fermions of two kinds, showed that the SRC pairs are predominantly unlike-fermion pairs [5–9]. These experiments were done using very different Fermi systems: protons and neutrons in atomic nuclei [8, 9] and two-spin state ultra-cold atomic gasses [5], which span more than 15 orders of magnitude in Fermi energy from MeV to neV), and exhibit different short-range interactions (a strong tensor interaction in the nuclear systems [6, 10], and a tunable Feshbach resonance in the atomic system [5]).

The nuclear studies showed that in the symmetric ^4He and ^{12}C nuclei, every proton with momentum $300 < k < 600$ MeV/c has a correlated partner nucleon, with neutron-proton (np) pairs outnumbering proton-proton (pp) and, by inference, neutron-neutron (nn) pairs

by a factor of ≈ 20 [6, 7, 11]. A recent study showed that in asymmetric heavy nuclei with unequal numbers of the different fermions, high-momentum protons still disproportionately belong to np pairs [12]. This suggested a new feature: an inversion of the momentum sharing between the minority and majority components. This inversion is due to the short-range interaction, which populates the high-momentum tail with equal amounts of majority and minority fermions, thereby leaving a larger proportion of majority fermions to occupy low momentum states ($k < k_F$) (see Fig. 1).

For light asymmetric nuclei the simple concept described above can be illustrated by detailed microscopic calculations.

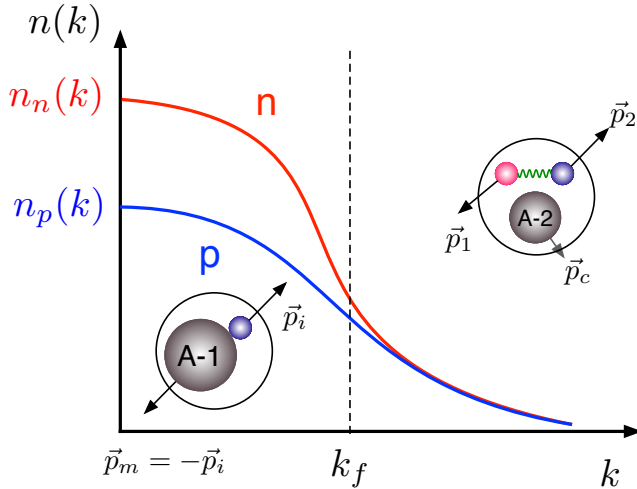


FIG. 1: Illustration of the momentum distribution of protons and neutrons in asymmetric nuclei. $n_n(k)$ and $n_p(k)$ are the neutron and proton momentum densities, respectively. The insets show the single nucleon in a mean field and the 2N-SRC pairs that dominate below and above k_F , respectively.

B. Energy Sharing in Light Nuclei ($A < 12$)

Detailed Variational Monte Carlo (VMC) calculations of the single-nucleon momentum distributions for a variety of symmetric and asymmetric light nuclei ($2 \leq A \leq 12$) are now available [13]. By integrating these single-nucleon momentum distributions one can obtain the average proton and neutron kinetic energies for different nuclei:

$$\langle T_p \rangle = \frac{\int_0^\infty n_p(k) (\sqrt{m_p^2 + k^2} - m_p) d^3k}{\int_0^\infty n_p(k) d^3k} \quad (1)$$

where $n_p(k)$ is the proton momentum distribution (and similarly for neutrons).

The average kinetic energy of the minority nucleons is larger than that of the majority nucleons in asymmetric nuclei and this effect increases with the nuclear asymmetry, see

Table I. This non-trivial result can be naturally explained by the dominance of neutron-proton pairs in the high momentum tail of the nuclear momentum distribution.

Nucleus	Asymmetry ($N - Z$)/ A	$\langle T_p \rangle$	$\langle T_n \rangle$	$\langle T_p \rangle / \langle T_n \rangle$
^8He	0.50	30.13	18.60	1.62
^6He	0.33	27.66	19.60	1.41
^9Li	0.33	31.39	24.91	1.26
^3He	-0.33	14.71	19.35	0.76
^3H	0.33	19.61	14.96	1.31
^8Li	0.25	28.95	23.98	1.21

TABLE I: The proton and neutron average kinetic energies as extracted from ab-initio VMC single-nucleon momentum distribution calculations [13]. The average kinetic energy of the minority nucleons is larger than that of the majority nucleons. This difference increases with the nuclear asymmetry [14].

We propose here to measure the momentum distribution of protons in the most asymmetric stable nuclei, ^3He and ^3H , and demonstrate that the minority (protons in ^3H) have average kinetic energy higher than the majority (protons in ^3He). The $A = 3$ nuclear system is a unique laboratory for such a study as discussed below.

C. Why ^3He and ^3H ?

The $A = 3$ system is the lightest and simplest asymmetric nuclear system. We can use the fact that that ^3He and ^3H are mirror nuclei to measure the difference between the momenta carried by majority (n in ^3H and p in ^3He) and minority (p in ^3H and n in ^3He) fermions by measuring $^3\text{He}(e, e'p)$ and $^3\text{H}(e, e'p)$. By isospin symmetry, we expect the proton momentum distribution in ^3H to equal the neutron momentum distribution in ^3He and vice versa. This avoids the difficulties and inaccuracies due to detecting neutrons.

Nucleon ground state momentum distributions cannot be directly measured; we can only measure missing-momentum distributions which represent a convolution of ground state momentum distributions and final state interaction effects. However, by measuring the relatively simple $A = 3$ nuclei we can (a) choose kinematics that minimize the effects of FSI

(see Section IG) and (b) calculate the relatively small correction due to FSI (see section IG).

There are no measurements of neutron momentum distributions in ^3He or of neutron or proton momentum distributions in ^3H .

We therefore propose to measure the majority and minority momentum distributions and their ratio with high accuracy by measuring the quasielastic knock-out of protons from ^3He and ^3H . Since there are many more calculations of ^3He , we will show plots of neutron and proton distributions in ^3He rather than proton distributions in ^3H and ^3He .

Fig. 2 shows the nucleon momentum distribution in the deuteron and the proton and neutron momentum distribution in ^3He calculated by [15–17] using the Argonne V18 (AV18) NN potential for the deuteron and Variational Monte Carlo (VMC) calculations using the Argonne V18 + Urbana IX (AV18+UIX) Hamiltonian [15, 18] for ^3He . The proton momentum distribution in ^3He is significantly greater than that of the neutron at low momenta but is approximately the same for $1.5 \leq k \leq 2.5 \text{ fm}^{-1}$ (corresponding to $300 \leq p \leq 500 \text{ MeV/c}$). Fig. 2 also shows the same quantities calculated by Alvioli *et al.* [19].

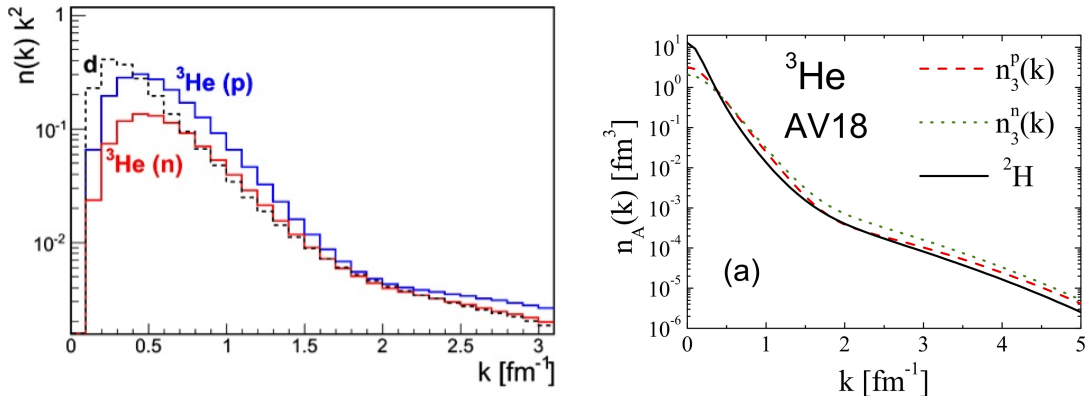


FIG. 2: The momentum distributions of the proton and the neutron in ^3He and in deuterium. Left: $k^2 n(k)$ from [15–18]. The proton’s momentum distribution integral is normalized to $Z = 2$ and the neutron’s to $N = 1$. The deuterium distribution is multiplied by $a_2(^3\text{He}/d) = 2$, the ratio of the cross sections for $^3\text{He}(e, e')$ to $d(e, e')$ at $1.5 \leq x \leq 2$ [9]. Right: $n(k)$ from [19]. The integrals of the momentum distributions are normalized to one.

For momenta $300 \leq p \leq 500 \text{ MeV/c}$, the nucleon momentum distributions in ^3He , ^3H , and the deuteron are all similar and dominated by np Short Range Correlations (SRC). At higher momenta (beyond the range of this experiment) the proton momentum distribution in ^3He increases relative to that of the neutron due to three-nucleon-correlations (e.e., ppn in ^3He).

The naive nucleon-counting expectation is that the cross section ratio of ${}^3\text{He}(e, e'p)$ to ${}^3\text{H}(e, e'p)$ will equal two, the ratio of protons/neutrons in ${}^3\text{He}$. However as shown in Fig. 3, the calculated ratio decreases rapidly from about three at low-momentum to about one at high momentum. Thus, by moving equal numbers of protons and neutrons from the low momentum to the high momentum regions, the correlations increase the low momentum ratio from two to three and decrease the high momentum ratio from two to one.

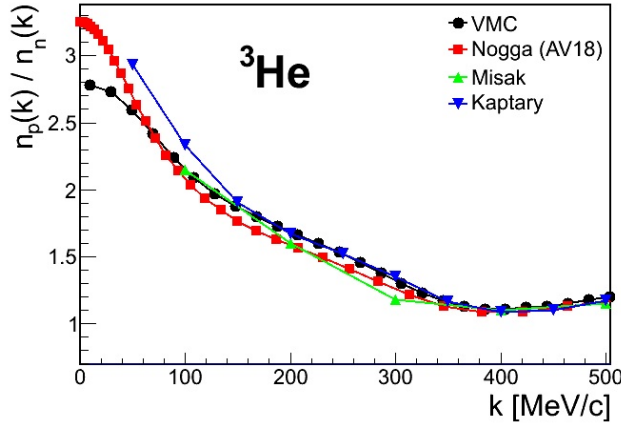


FIG. 3: The calculated ratio of proton to neutron momentum distributions in ${}^3\text{He}$. This corresponds to the ratio of momentum distributions for ${}^3\text{He}(e, e'p)$ to ${}^3\text{H}(e, e'p)$.

The correlations also change the relative kinetic energies of protons in ${}^3\text{He}$ and ${}^3\text{H}$ (i.e., of the majority and minority nucleons in the $A = 3$ system). We calculate the build-up of the average kinetic energy of the proton (or neutron) up to some momentum k as

$$\langle T_p \rangle_0^k = \frac{\int_0^k n_p(k') (\sqrt{m_p^2 + k'^2} - m_p) d^3k'}{\int_0^\infty n_p(k') d^3k'} \quad . \quad (2)$$

The majority (p in ${}^3\text{He}$) and minority (p in ${}^3\text{H}$) average kinetic energies and their ratio are shown in Fig. 4. Integrated up to momenta of about 150 MeV/c, the majority have more kinetic energy; integrated up to higher momenta the ratio is inverted and the minority have more kinetic energy.

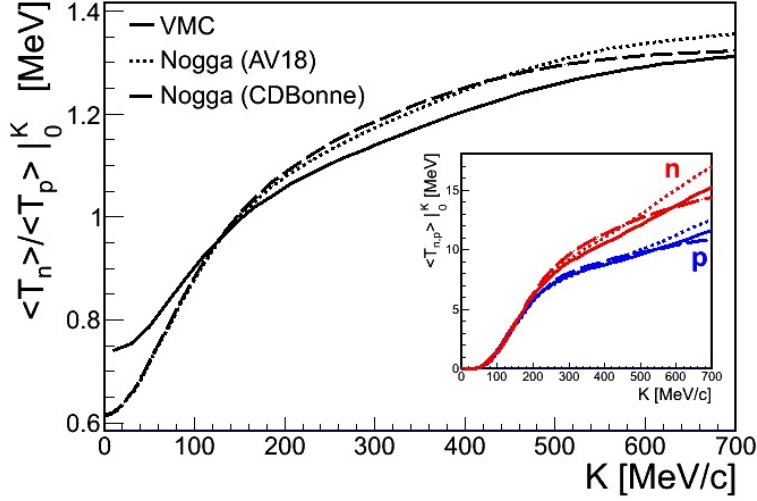


FIG. 4: The ratio of the neutron to proton average kinetic energy in ${}^3\text{He}$ integrated up to momentum k as in Eq. 2. Inset: The average kinetic energy per neutron (blue) and per proton (red) in ${}^3\text{He}$ integrated up to momentum k . The neutron in ${}^3\text{He}$ corresponds to our proposed measurement of ${}^3\text{H}(e, e'p)$.

As we will discuss below, we can measure the ${}^3\text{He}(e, e'p)$ and ${}^3\text{H}(e, e'p)$ cross sections and their ratio very accurately. We can use the ratio to very reliably extract the ratio of ground state minority to majority nucleon momentum distributions in $A = 3$ nuclei and the ratio of minority to majority average kinetic energy with very small sensitivity to FSI.

D. Relevance to other fields

In the symmetric ${}^4\text{He}$ and ${}^{12}\text{C}$ nuclei, every proton with momentum $300 < k < 600$ MeV/c (where $k_F \approx 220$ MeV/c) has a correlated partner nucleon with neutron-proton (np) pairs outnumbering proton-proton (pp), and by inference neutron-neutron (nn), pairs by a factor of ≈ 20 [6, 7, 11]. In a paper submitted to Science we present data from Hall B analyzed as part of the data mining project [12]. We show, for the first time, the identification of SRC pairs in the high-momentum tail of nuclei heavier than carbon and with more neutrons than protons (i.e., $N > Z$). This publication demonstrates clearly the universal nature of SRC pairs, which even in heavy imbalanced nuclei such as lead ($N/Z = 126/82$) are still dominated by np pairs (see Fig. 5). This np -dominance causes a greater fraction of protons than neutrons to have high momentum in neutron-rich nuclei, thereby inverting the momentum sharing in imbalanced nuclei.

The np -dominance of SRC pairs and the resulting inversion of the momentum sharing in heavy neutron rich imbalanced nuclei have wide ranging implications in astro, nuclear and particle physics. These include the determination of the density dependence of the nuclear symmetry-energy up to supra-nuclear densities [20–24], analysis of neutrino-nucleus

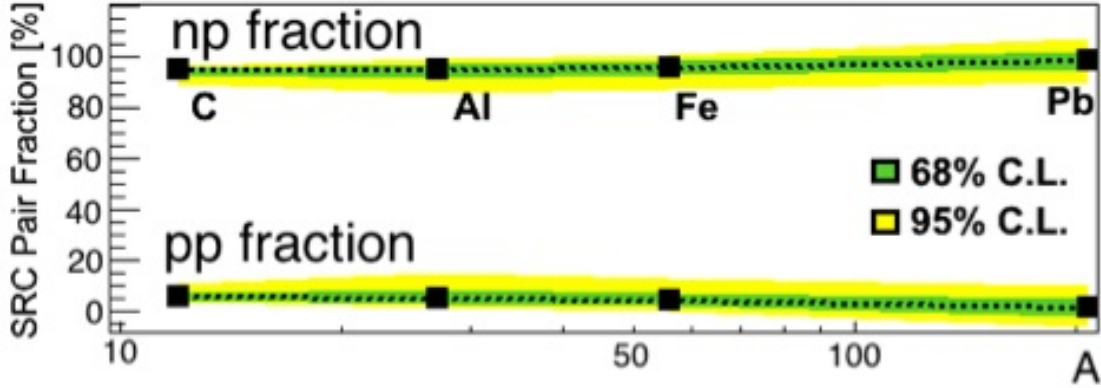


FIG. 5: The fraction of np (top) and pp (bottom) SRC pairs. The green and yellow bands reflect 68% and 95% confidence levels. np -SRC pairs dominate over pp -SRC in all measured nuclei.

scattering data for the determination of the nature of the electro-weak interaction [25, 26], and the isospin dependence of the EMC effect as a cause of the standard-model NuTeV anomaly [27–31].

One application is in neutrino physics where most experiments still use a simple relativistic Fermi gas model to describe the nucleus. Recent high precision measurements of charged current quasi-elastic neutrino-nucleus scattering cross-sections [25, 26] show the need to include the effects of np -SRC pairs in both their reaction model and detector response. This is expected to be a crucial ingredient in facilitating the precision requirements of next generation neutrino experiments [32].

The NuTeV anomaly is a three standard deviation difference from the Standard Model prediction in the extraction of the electroweak-mixing (Weinberg) angle from neutrino deep inelastic scattering from iron [30]. This anomaly might be due to an Isospin dependent EMC effect in iron [31]. The EMC effect implies modification of bound nucleon structure [33] and was recently shown to linearly correlate with the number of SRC (high momentum) pairs in nuclei [29]. If the EMC nucleon modification is dominated by high momentum nucleons and protons have higher momentum than neutrons in heavy asymmetric nuclei, then this would provide an alternative model [31] for an Isospin dependent EMC effect which can quantitatively explain the NuTeV anomaly.

The nuclear symmetry energy describes how the energy per nucleon in nuclear matter changes as a function of the proton fraction. While its value at the nuclear saturation density is relatively well constrained [24], its density dependence is not, largely due to uncertainties

in the tensor component of the nucleon-nucleon interaction [22, 23]. Knowledge of this density dependence at supra-nuclear densities is important for different aspects of nuclear astrophysics and in particular neutron stars [24]. Recent calculations show that the inclusion of high-momentum tails, dominated by tensor force induced np -SRC pairs, dramatically softens the nuclear symmetry energy at supra-nuclear densities [20–23].

Generalizing our results to other systems, the behavior of two component Fermi systems that interact with a large scattering length is constrained by universal relations which involve “the contact”, a measure of the number of short distance unlike-fermion pairs [1–3]. Recent experiments with symmetric two-spin-state ultra-cold atomic gases measured the contact.

This measurement will not measure a specific parameter needed for these different systems. However, it will contribute to our general understanding and will help constrain the theories common to this measurement and to these systems.

E. Impact on the 12 GeV JLab program

The results of this proposed measurement will complement other 12 GeV JLab experiments, particularly EMC effect measurements of light nuclei and inclusive (e, e') measurements of light nuclei.

E12-11-112 will measure inclusive electron scattering, (e, e') , from ^3He and ^3H from $x_B \approx 0.7$ to $x_B = 3$, covering the resonance, quasielastic, and $x_B > 1$ regions. Inclusive electron scattering at $x_B > 1$ is sensitive to the integral of the nuclear momentum distribution from some threshold momentum to infinity, where the threshold momentum increases with x_B . Exclusive $(e, e'p)$ cross sections are sensitive to the momentum distribution $n(p)$ at $p \approx p_{miss}$. Thus, our proposed $(e, e'p)$ exclusive electron scattering measurement will complement the inclusive measurements. In addition, the theoretical uncertainties of the exclusive measurements will be very different from those of inclusive measurements. As this will be our only opportunity to study ^3H at Jefferson Lab, it is important to perform both experiments.

The EMC effect is the deviation from unity of the per-nucleon deep inelastic scattering (DIS) cross section of nucleus A relative to deuterium. The EMC effect cannot be explained by purely nucleonic effects (e.g., nucleon motion and binding energy) and therefore implies that nucleons are modified in nuclei [33].

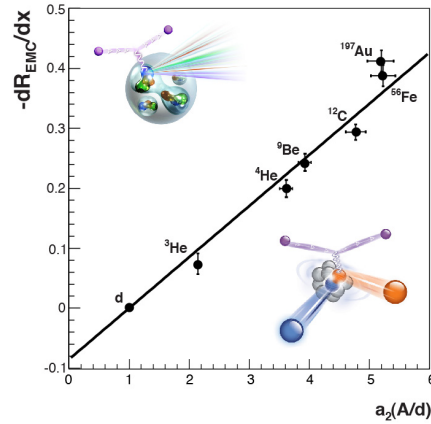


FIG. 6: Linear correlation between the strength of the EMC effect and the amount of 2N-SRC in nuclei [34].

The magnitude of the EMC effect is directly proportional to the number of SRC pairs [29, 34] (see Fig. 6) and thus the EMC effect is associated with large momentum (large virtuality) nucleons in nuclei.

The MARATHON experiment will measure the ratio of DIS cross sections in ^3He and ^3H to determine the ratio of F_2^p/F_2^n . They expect that off-shell effects due to the modification of the bound nucleon structure will be small. However, since models predict that the modification of the bound nucleon structure function is proportional to nucleon virtuality [33] and since protons in ^3H are expected to have higher momentum than protons in ^3He , this means that F_2^p will not be the same in ^3He and ^3H (and similarly for neutrons and F_2^n).

By directly measuring the proton (and by inference the neutron) momentum distributions in ^3He and ^3H , this experiment will provide information to help correct the MARATHON data for possible off-shell effects.

F. Previous Measurements

The most direct way of studying nucleon momentum distributions in nuclei is to measure the quasi-elastic (QE) $^3\text{He}(e, e'p)$ and $^3\text{H}(e, e'p)$ reactions as a function of missing momentum, $\vec{p}_m = \vec{q} - \vec{p}_p$, where \vec{p}_p is the momentum of the outgoing, observed proton and \vec{q} is the momentum transfer. The missing momentum \vec{p}_m equals \vec{p}_r , the momentum of the $A - 1$ recoil. Within the Plane Wave Impulse Approximation (PWIA) where Final State Inter-

actions (FSI) are neglected, $\vec{p}_{init} = -\vec{p}_m$ where \vec{p}_{init} is the initial momentum of the target nucleon before the interaction.

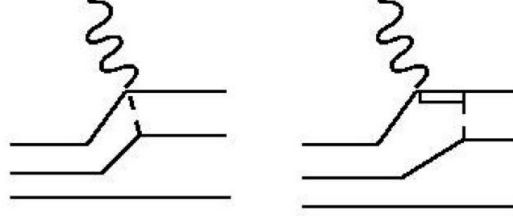


FIG. 7: Diagrams for Meson Exchange Currents (left) and Isobar Configurations (right).

However, depending on the selected kinematics, other reaction mechanisms can contribute to the cross section. The outgoing (struck) proton can rescatter from the other nucleons (FSI), or the virtual photon can couple to the exchanged meson (MEC) or the virtual photon can excite the nucleon to an intermediate Δ isobar state (IC). Fig. 7 shows schematically how IC and MEC can cause the measured missing momentum to be different from the genuine ground state momentum distribution.

Due to these competing reaction channels, previous experiments at $Q^2 < 1$ (GeV/c)² [35–39] did not strongly constrain the high momentum components of the ground state momentum distribution. The Jefferson Lab $^3\text{He}(e, e'p)$ measurement was performed in kinematics such that the cross sections measured at high-missing-momentum ($p_m \geq 300$ MeV/c) were dominated by FSI (see Figs. 8 and 9) [39, 40]. The FSI domination is shown by the significant disagreement between PWIA calculations and the measured cross sections and by the relative agreement between calculations including FSI and those same cross sections. This FSI domination is not surprising, because small angle rescattering of the knocked-out proton contributes significantly at some kinematics.

The only previous measurement on $^3\text{H}(e, e'p)$ dates from 1964 [45]. Unfortunately, little can be learned about the proton momentum distributions in ^3H from this measurement, due to its low momentum transfer and limited statistics (see Fig. 10).

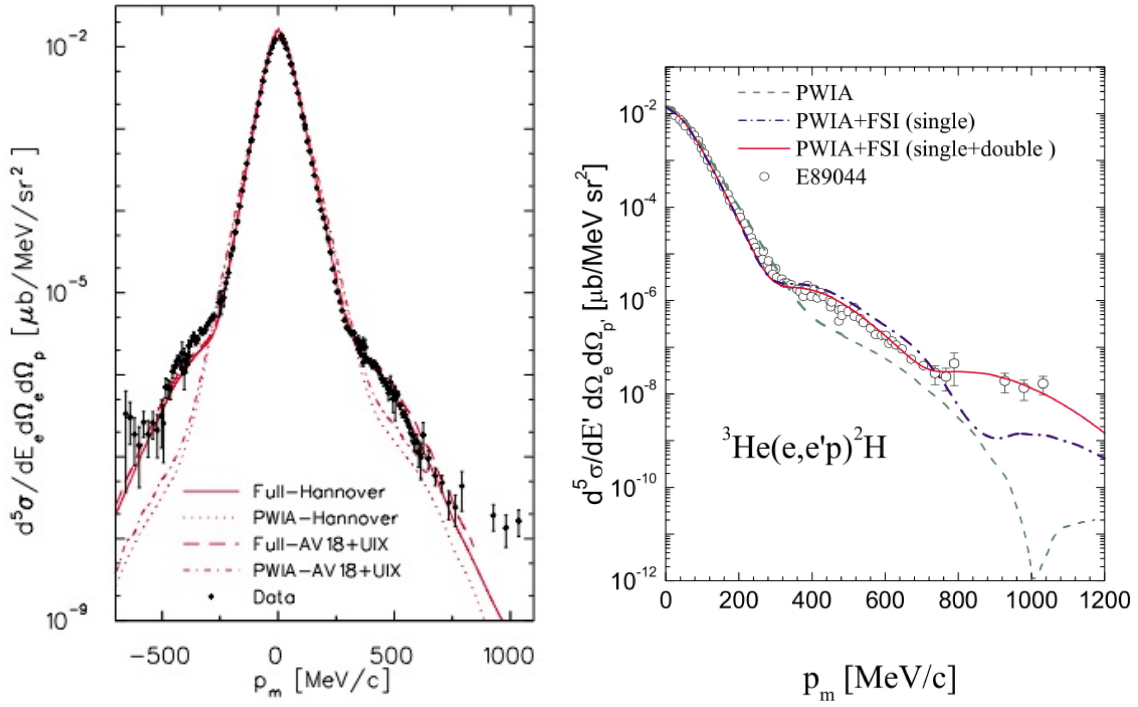


FIG. 8: The measured ${}^3\text{He}(e, e'p){}^2\text{H}$ cross section as a function of the missing momentum p_m . The left figure also shows PWIA and full calculations in the diagrammatic approach by Laget for two different ground state wave functions (see [39] and references therein). The right figure shows the same data with calculations by Ciofi degli Atti and Kaptari [41]. The dashed line corresponds to the PWIA, the dot-dashed line includes FSI with single rescattering and the solid line includes both single and double rescattering [41].

G. Minimizing Final State Interactions

Fortunately, measurements on the deuteron show that we can select kinematics to minimize the effects of FSI [46]. Fig. 11 shows that the impact of FSI on the cross section decreases rapidly as θ_{rq} , the angle between the recoil momentum ($\vec{p}_{recoil} = \vec{p}_m$) and \vec{q} in the laboratory frame, decreases from 75° to 35° .

We expect the same FSI suppression to hold for the nucleons in the correlated pair in ${}^3\text{He}$ and ${}^3\text{H}$. Calculations by Ciofi degli Atti [47] and by Sargsian [48] show that FSI are minimized at smaller values of θ_{rq} . Fig. 12 shows that the effects of FSI peak at $\theta_{rq} \approx 70^\circ$ and are much smaller for $\theta_{rq} \leq 40^\circ$.

Fig. 13 shows the calculated ratio of the FSI to PWIA ${}^3\text{H}$ and ${}^3\text{He}(e, e'p)$ cross sections for a range of missing energies and missing momenta at a recoil angle $\theta_{rq} = 30^\circ$. The ratios are almost all reasonably close to unity.

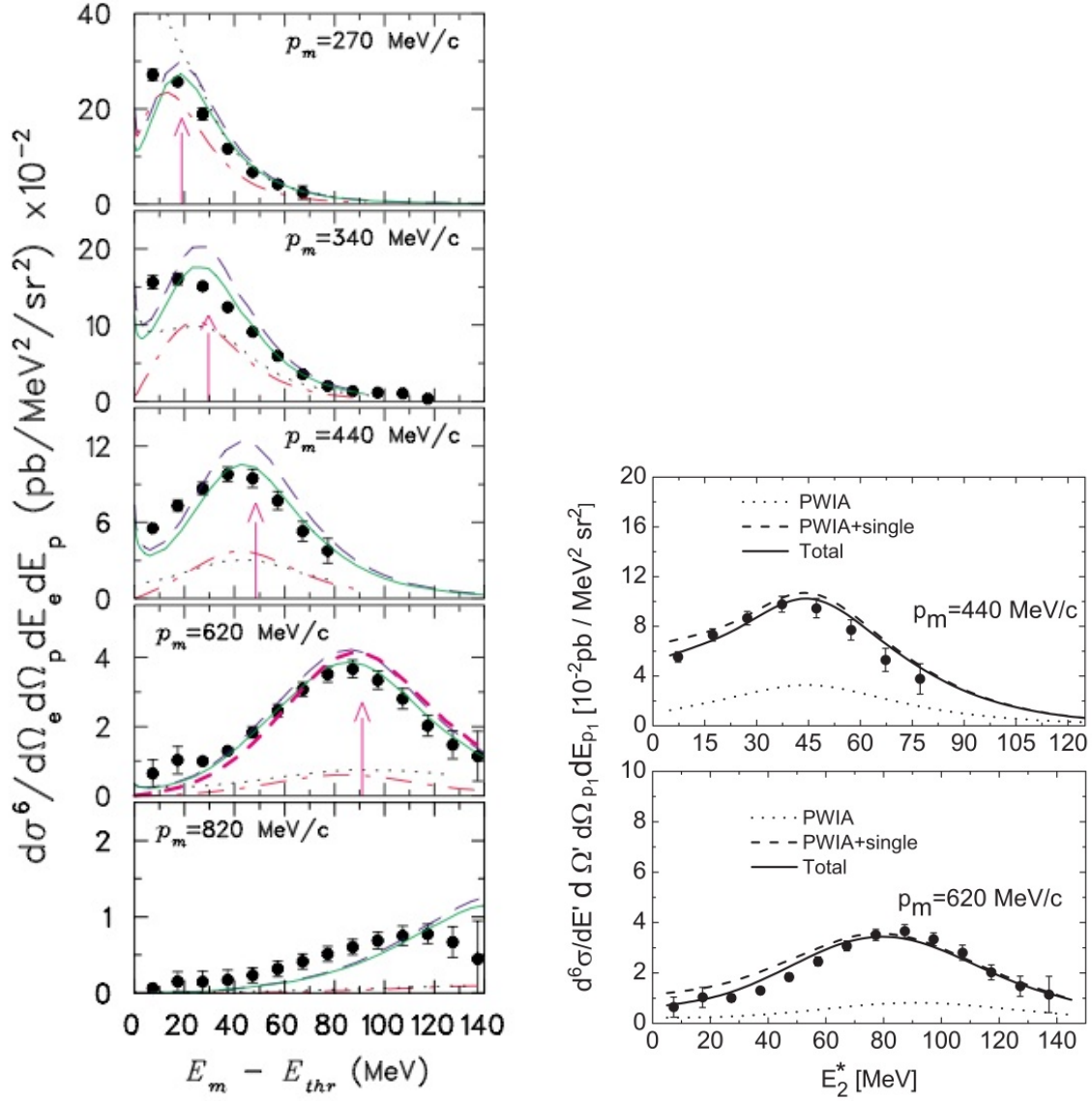


FIG. 9: (left) The cross section for the ${}^3\text{He}(e, e'p)pn$ reaction as a function of missing energy [40]. The vertical arrow gives the peak position expected for disintegration of correlated pairs, $E_m = \omega - T_p - T_r = p_m^2/4m$ (where T_p is the kinetic energy of the detected proton and $T_r = p_m^2/2m_{A-1}$ is the kinetic energy of the recoiling $A-1$ “nucleus”). The black dotted curve presents a PWIA calculation using Salme’s spectral function and σ_{ce1} electron-proton off-shell cross section and the red dash-dotted line is a Laget PWIA calculation. Other curves are Laget’s calculations for PWIA+FSI (black long dashed line) and his full calculation (solid green line), including meson-exchange currents and final-state interactions. In the 620 MeV/c panel, the additional bold red short dashed curve is a calculation with PWIA + FSI only within the correlated pair [42, 43]. (right) The same experimental cross section plotted vs $E_2^* = E_m - E_{thr}$ compared to the unfactorized calculations of Alvioli, Ciofi degli Atti and Kaptari [44]. The dotted line shows the PWIA calculation, the dashed line includes FSI with single rescattering and the solid line includes FSI with both single and double rescattering.

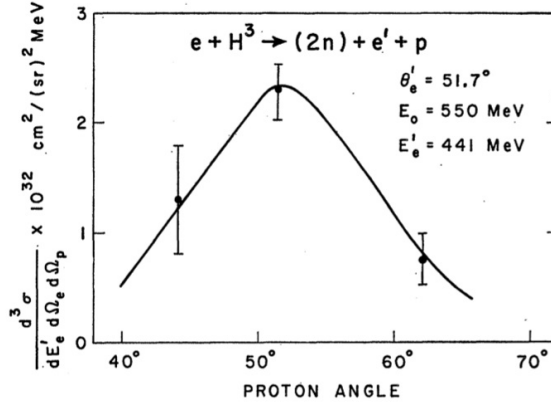


FIG. 10: The cross section for ${}^3\text{H}(e, e'p)$ as a function of proton angle [45].

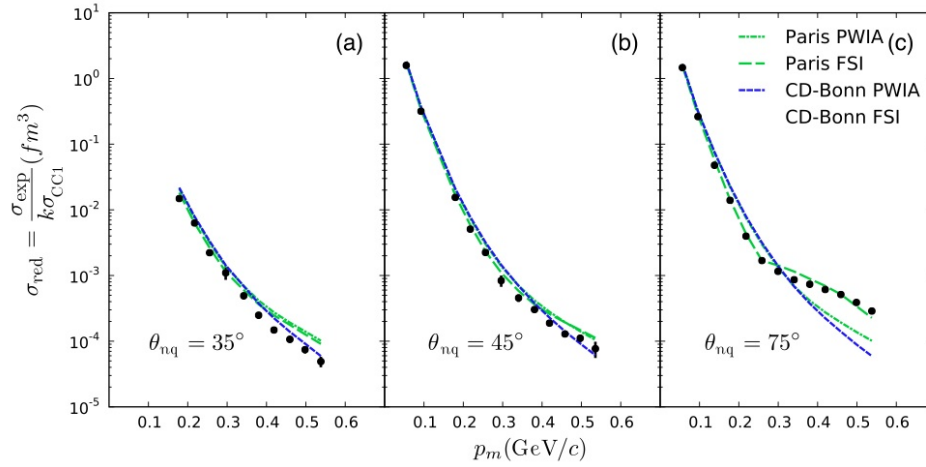


FIG. 11: The reduced cross section for $d(e, e'p)$ as a function of missing momentum for three different lab recoil angles, (a) $\theta_{rq} = 35^\circ$, (b) $\theta_{rq} = 45^\circ$, and (c) $\theta_{rq} = 75^\circ$. All calculations are by M. Sargsian [46].

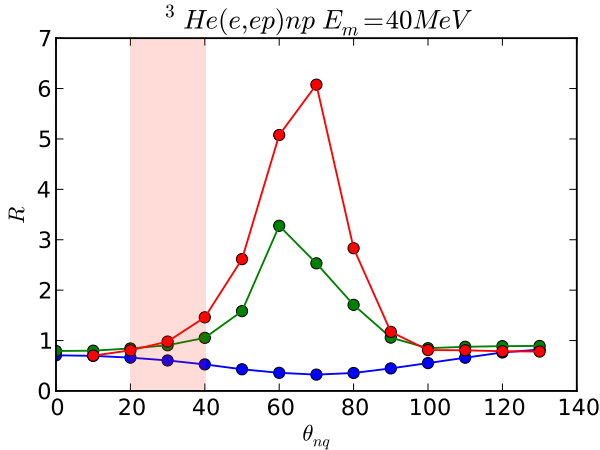


FIG. 12: The calculated ${}^3\text{He}(e, e'p)$ ratio of the cross section which includes rescattering of the struck nucleon (FSI) to the PWIA cross section for $p_m = 0.2$ (blue), 0.4 (green), and 0.5 (red) GeV/c as a function of θ_{rq} , the angle between the recoil momentum and \vec{q} in the laboratory frame [48]. The tan band indicates the angles for the measurements proposed here.

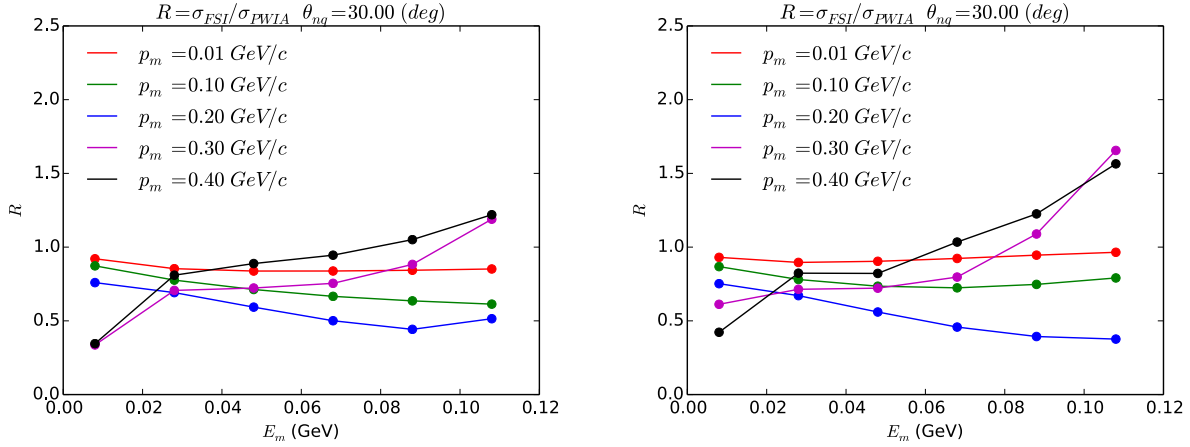


FIG. 13: The ratio of the FSI calculation which includes rescattering of the struck nucleon to the PWIA cross section as a function of missing energy $E_m = \omega - T_p - T_r$ for $\theta_{rq} = 30^\circ$ and for various missing momenta as calculated by Sargsian [48]. Left: ${}^3\text{H}$; Right: ${}^3\text{He}$.

We will significantly reduce the remaining effects of FSI by forming the ratio of ${}^3\text{He}(e, e'p)$ to ${}^3\text{H}(e, e'p)$. In the simplest picture, the struck proton has the same probability to rescatter from the other two nucleons whether it was knocked out of ${}^3\text{He}$ or ${}^3\text{H}$.

Calculations by Sargsian at our proposed kinematic settings of $Q^2 = 2 \text{ (GeV/c)}^2$ and $\theta_{rq} = 30^\circ$ show that the effects of FSI almost entirely cancel in the ratio of ${}^3\text{He}(e, e'p)$ to ${}^3\text{H}(e, e'p)$ cross sections (see Fig. 14).

II. THE MEASUREMENT

We propose to measure the ${}^3\text{He}(e, e'p)$ and ${}^3\text{H}(e, e'p)$ cross sections for $0 \leq p_m \leq 500 \text{ MeV/c}$ using the MARATHON target and the Hall A HRS spectrometers in their standard configuration in order to extract information about the ground state momentum distributions.

The MARATHON target has four identical 25-cm sealed-cell gas target cells, with a maximum room-temperature pressure of 200 psi for T_2 and 400 psi for H_2 , D_2 and ${}^3\text{He}$ (see Fig. 15). Each target cell is sealed and is cooled during target operation. The open cell design allows a wide range of scattering angles. The wall thickness is 0.018" Al (120 mg/cm²) and the entrance and exit windows are 0.010" Al (65 mg/cm²). The target can withstand a maximum beam current of 25 μA . The monatomic ${}^3\text{He}$ and diatomic ${}^3\text{H}$ (T_2) targets will have the same thickness (82 mg/cm²) and number density. This gives a maximum

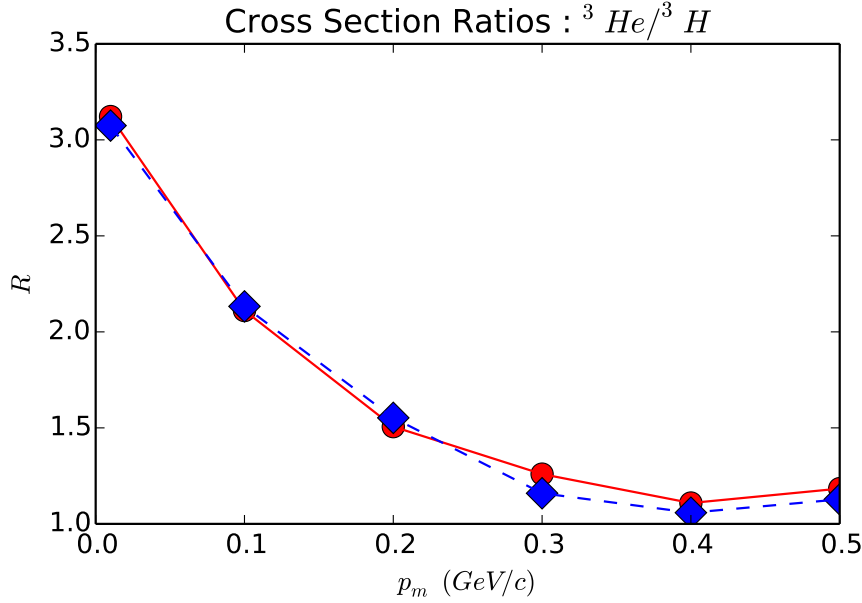


FIG. 14: The ratio of the ${}^3\text{He}(e, e'p)$ to ${}^3\text{H}(e, e'p)$ cross sections integrated over missing energy at $Q^2 = 2$ (GeV/c) 2 and $\theta_{rq} = 30^\circ$ for PWIA calculations (red solid curve) and FSI calculations (blue dashed curve) by Sargsian [48].

luminosity of 7.4×10^{36} nucleons/(cm 2 ·s), much less than the maximum Hall A luminosity of 10^{39} nucleons/(cm 2 ·s). At this low luminosity, backgrounds and other rate-related effects should be negligible. The proton spectrometers will not see the entrance and exit windows.

In order to minimize the effects of competing reaction channels (MEC, IC, and FSI) and to maximize our sensitivity to the ground state momentum distribution, we will measure at

- high Q^2 ($Q^2 \approx 2$ (GeV/c) 2)
- $x = Q^2/2m\omega > 1$
- small θ_{rq} ($\theta_{rq} < 40^\circ$)

In addition, we will measure the different nuclei at identical kinematic settings with the identical experimental setup. This will make it possible to probe the genuine momentum distributions with significantly smaller experimental and theoretical corrections and hence uncertainties.

Since, at fixed Q^2 , cross sections increase with beam energy, we will measure the cross section with two-pass beam, $E_0 = 4.4$ GeV. This is the highest beam energy we can use and still detect the scattered electron in the Hall A HRS.

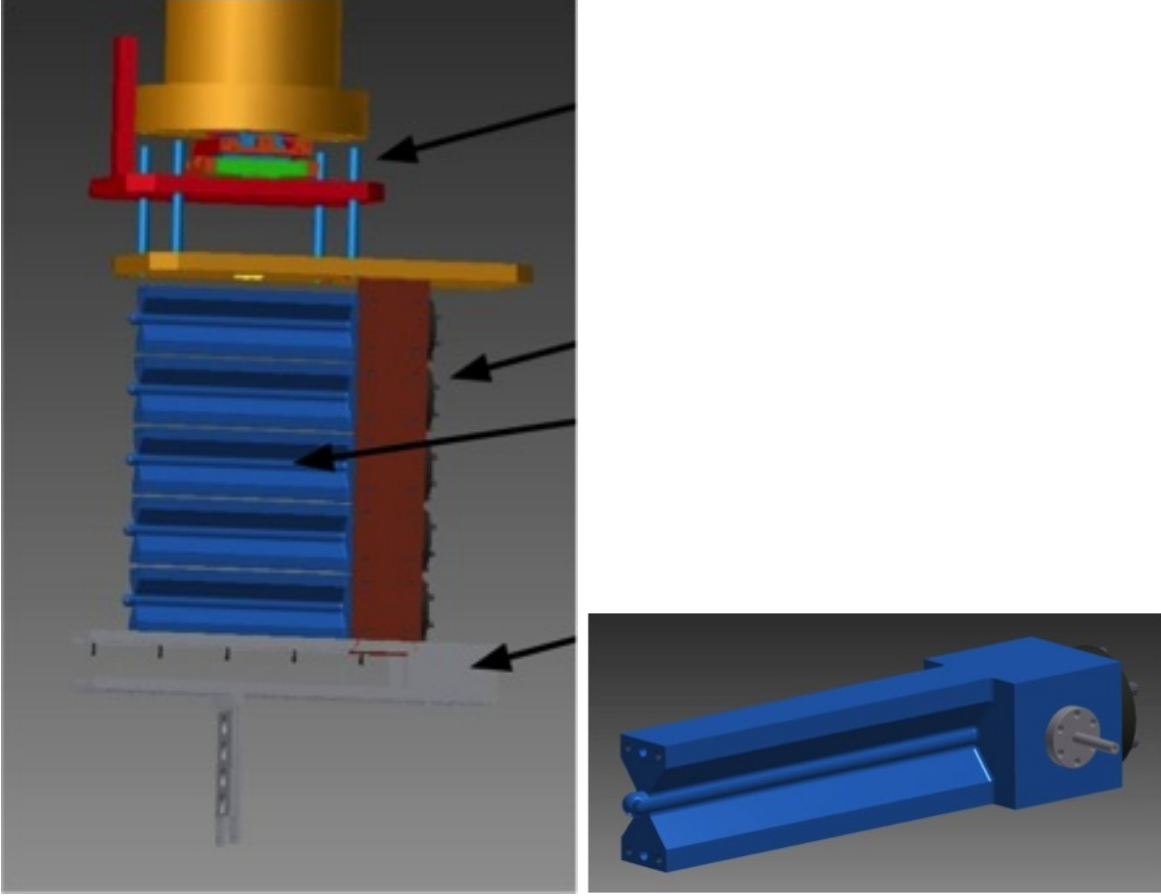


FIG. 15: The MARATHON target. (left) The four identical gas target cells are shown in blue and the optics target and solid targets are shown in grey. The beam is incident from the right. (right) A detailed view of one target cell.

As Q^2 increases, the cross section decreases and the effects of IC and MEC decrease. In addition, the accuracy of the Eikonal approximation for calculating the effects of FSI increases. We will measure at $Q^2 = 2 \text{ (GeV/c)}^2$ as a compromise between decreasing cross section and increasing ease of interpretation.

Based on deuteron results [46] and ^3He calculations [47, 48], we plan to reduce the effects of FSI on the cross sections by measuring the $(e, e'p)$ reaction at an angle of approximately $\theta_{rq} \approx 30^\circ$ between the nuclear recoil and the momentum transfer.

Due to the small Z of the target nuclei, radiative effects will be significantly smaller than in previous Hall A $(e, e'p)$ measurements of ^{16}O and ^{208}Pb . They will further cancel in the ratio of the ^3He and ^3H cross sections. Coulomb corrections will be similarly small. Radiative effects will be calculated using the standard Hall A methods of $(e, e'p)$ experiments.

We selected the central angle and momentum of the detected electron and knocked-out

proton according to 2-body kinematics for proton knockout from a deuteron. For $A = 3$ targets, this centers the kinematics close to the SRC missing energy peak where the cross section is maximum (see Fig. 9). It also ensures that we will measure both the two-body-break-up and three-body-break-up channels of ${}^3\text{He}(e, e'p)$.

The minimum in the ${}^3\text{He}(e, e'p)$ to ${}^3\text{H}(e, e'p)$ cross section ratio (i.e., where NN -SRC dominate) should be at about 0.4 GeV/c (see Fig. 3). We will measure the ${}^3\text{He}/{}^3\text{H}$ ratio out to $p_m \approx 0.5$ GeV/c. Table II shows the kinematic settings to cover this range of missing momentum.

We request one day of commissioning and calibration time to measure spectrometer optics, pointing, ${}^1\text{H}(e, e'p)$, and one low- p_{miss} ${}^3\text{He}(e, e'p)$ data point to overlap with Refs. [39, 40]. We expect that the systematic uncertainties due to errors in beam energy, beam charge measurements, detector efficiencies and target thickness will be very similar to the 4.5% reported in [46] for $d(e, e'p)$.

$\langle p_m \rangle$ (MeV/c)	x	E_e (GeV)	θ_e	p_p (GeV/c)	θ_p	total beam time (days)
	Calibration and commissioning					1
100	1.15	3.47	20.86°	1.607	48.67°	1
300	1.41	3.64	20.35°	1.352	58.55°	8
	Total beam time request					10

TABLE II: The central kinematics and beam time for each setting. The beam energy is 4.4 GeV and $Q^2 = 2.0$ (GeV/c)² for all settings.

A. MCEEP Simulations

We calculated cross sections and rates using the deuteron PWIA cross section integrated over the experimental acceptances using MCEEP, including radiative corrections. We used the parameters of the MARATHON target, with a 25-cm long target cell, a deuterium target density of 75 mg/cm², and a maximum beam current of 25 μA . The ${}^3\text{He}$ and ${}^3\text{H}$ targets will have approximately the same mass density as the deuterium target and will therefore have about 2/3 of the number density. We expect the ${}^3\text{He}(e, e'p)$ and ${}^3\text{H}(e, e'p)$ cross sections to be at least twice as large as the $d(e, e'p)$ cross section at large missing

momenta, compensating for the decreased number density of the ^3He and ^3H targets and for other expected experimental inefficiencies.

The yields as a function of missing momentum are shown in Fig. 16 for the three kinematic points. Figs. 17 and 18 show the distribution of events.

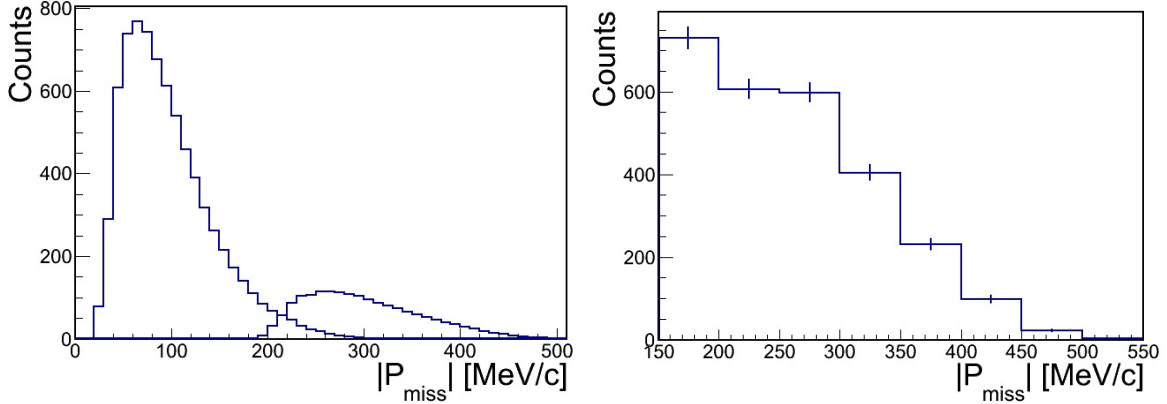


FIG. 16: (left) The expected number of events as a function of missing momentum for the kinematic points of Table II; (right) the number of events for all kinematic points combined, starting at $p_m = 150$ MeV/c.

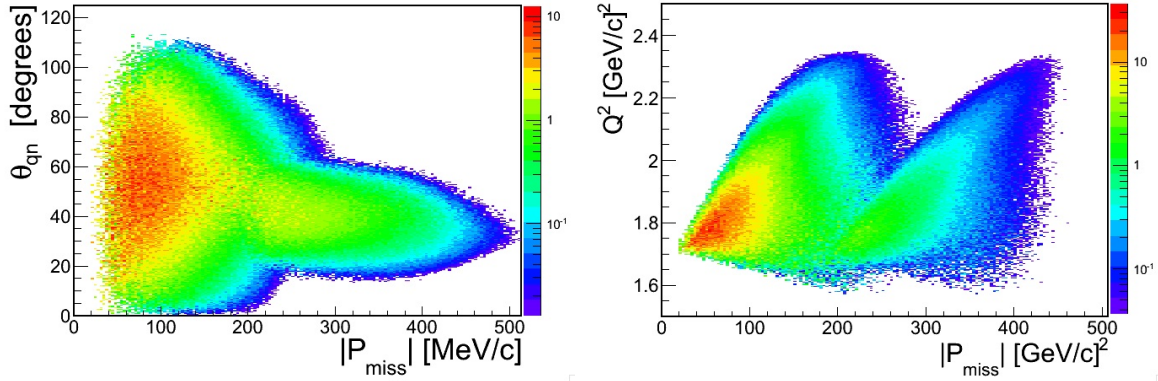


FIG. 17: (left) θ_{rq} , the angle between the recoiling system (missing momentum) and \vec{q} , versus the missing momentum. (right) Q^2 , the square of the momentum transfer plotted versus the missing momentum. The vertical scales are logarithmic.

B. Expected Results

We will measure the $^3\text{He}(e, e'p)$ and $^3\text{H}(e, e'p)$ cross sections at each value of missing momentum by integrating the cross sections over missing energy. We will then construct the

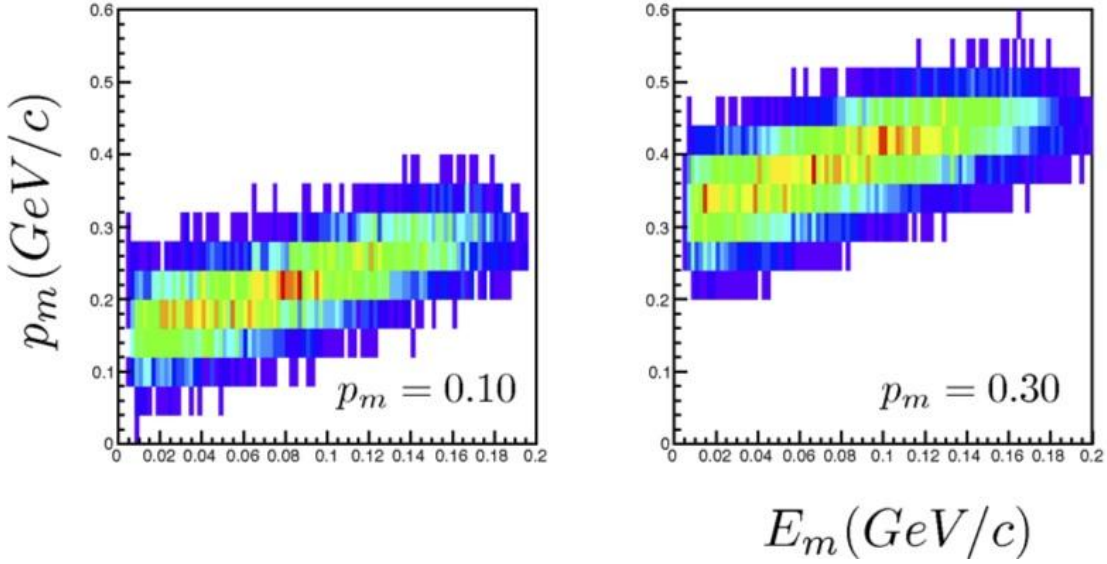


FIG. 18: The missing energy – missing momentum distribution for the two kinematic settings. This shows the kinematic coverage and does not include cross section weighting.

cross section ratio ${}^3\text{He}(e, e'p)/{}^3\text{H}(e, e'p)$. The expected statistical uncertainties are shown in Figs. 19 and 20. The expected results for the ratio of kinetic energies is shown in Fig. 21.

III. SUMMARY

Fully understanding few-nucleon systems is vital to our understanding of nuclear physics. We propose to take advantage of a unique opportunity to measure the cross sections of ${}^3\text{H}(e, e'p)$ and ${}^3\text{He}(e, e'p)$ in Hall A in order to determine the momentum distributions of the minority and majority fermions in asymmetric nuclei. ${}^3\text{H}(e, e'p)$ has never been measured before and ${}^3\text{He}(e, e'p)$ has never been measured in kinematics which minimize the effects of final state interactions (FSI), meson exchange currents, and isobar configurations.

By forming the cross section ratio of ${}^3\text{He}(e, e'p)$ to ${}^3\text{H}(e, e'p)$, the remaining effects of FSI almost entirely cancel, allowing us to extract the ratio of their momentum distributions with unprecedented precision. We propose to measure this ratio from $p_m = 0$ where independent nucleons dominate (where the effect of SRC increases the ratio from the naive expectation due to proton counting of two) to $p_m = 0.5$ GeV/c where nucleons belonging to short range correlations (SRC) dominate (and the naive ratio due to pair counting should be about one).

We also propose to measure the absolute cross sections of these reactions in order to

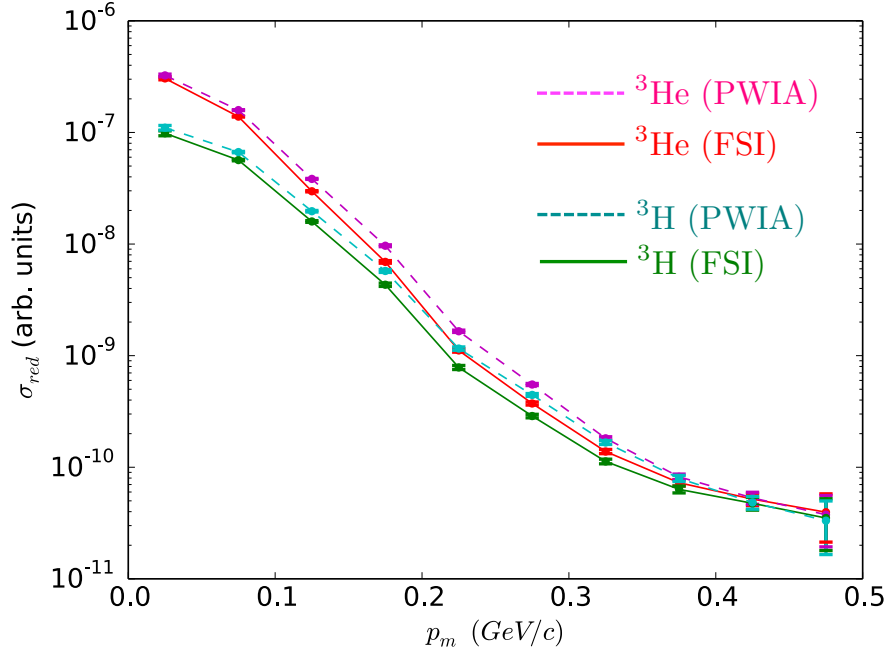


FIG. 19: The expected statistical uncertainties in the proposed measured reduced cross sections for $^3\text{He}(e, e'p)$ and $^3\text{H}(e, e'p)$ integrated over missing energy as a function of missing momentum. The results are shown for calculations both without (PWIA) and with (FSI) the effects of final state interactions [48].

provide a stringent test of theoretical models. These models will face different challenges in calculating the absolute cross sections and the cross section ratio $^3\text{He}(e, e'p)/^3\text{H}(e, e'p)$.

This will allow us to measure the majority and minority fermion momentum distributions in the most asymmetric stable nuclei. This will be a strong test of modern calculations in asymmetric nuclei.

This proposal was deferred by PAC 40. In this resubmission, we have reduced the requested beam time from 30 to 10 days by focussing on ^3He and ^3H , omitting the deuterium target and reducing the beam time at large missing momentum. We also emphasize the importance of measuring majority and minority fermion momentum distributions in asymmetric nuclei.

We propose to measure these cross sections using the MARATHON target and the Hall A HRS spectrometers in their standard configuration. Radioactive targets in general and tritium targets in particular pose serious safety issues and are thus very difficult to install. The MARATHON target will only be at Jefferson Lab for a brief period. This will be the

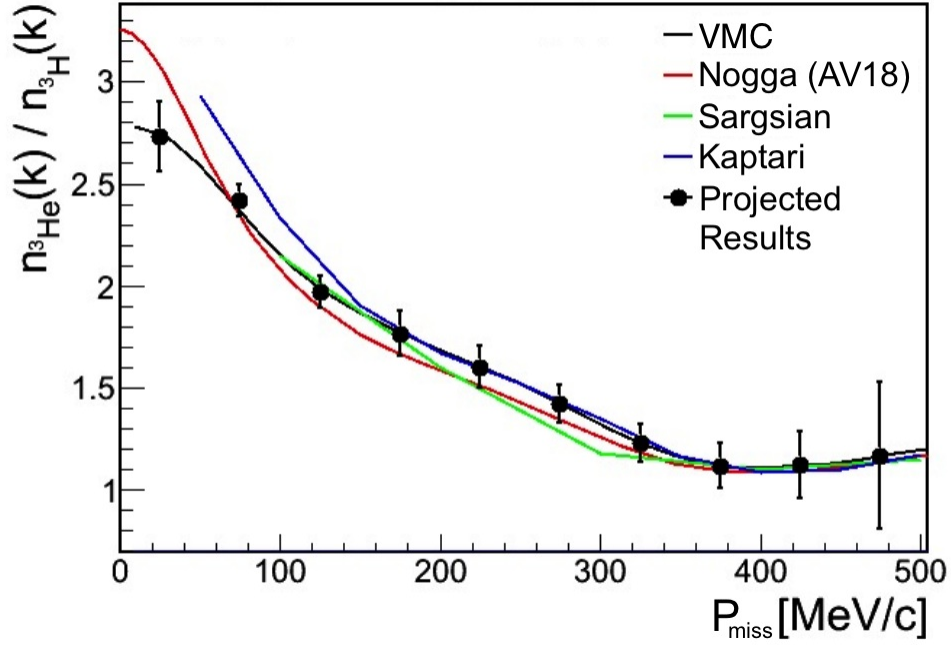


FIG. 20: The expected statistical uncertainties in the proposed measured cross section ratios of ${}^3\text{He}(e, e'p)/{}^3\text{H}(e, e'p)$ as a function of missing momentum.

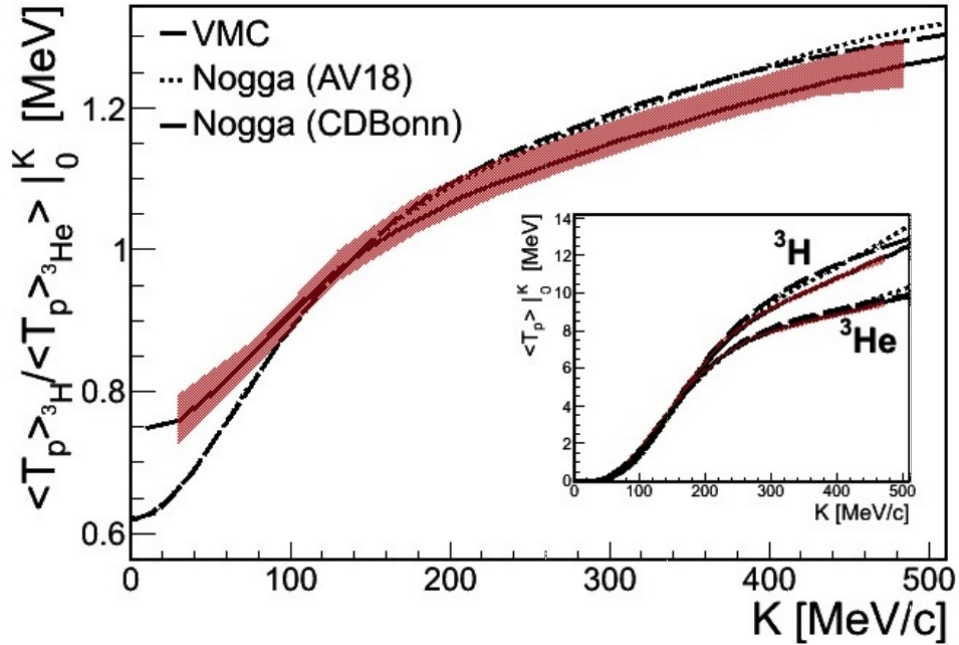


FIG. 21: The expected statistical uncertainties in the ratios of the average nucleon kinetic energies measured in ${}^3\text{He}(e, e'p)$ and ${}^3\text{H}(e, e'p)$ as a function of missing momentum (see Eq. 2). The red band shows the total expected uncertainty of the experimental integration.

only opportunity to measure ${}^3\text{H}(e, e'p)$. It is crucial to take advantage of this opportunity to fill a gaping hole in our knowledge of few-nucleon systems.

We request 10 days of beam time to measure ${}^3\text{H}(e, e'p)$ and ${}^3\text{He}(e, e'p)$.

-
- [1] S. Tan, *Annals of Physics* **323**, 2952 (2008).
 - [2] S. Tan, *Annals of Physics* **323**, 2971 (2008).
 - [3] S. Tan, *Annals of Physics* **323**, 2987 (2008).
 - [4] E. Braaten, in *The BCS-BEC Crossover and the Unitary Fermi Gas*, edited by W. Zwerger (Springer, Berlin, 2012).
 - [5] J. T. Stewart, J. P. Gaebler, T. E. Drake, and D. S. Jin, *Phys. Rev. Lett.* **104**, 235301 (2010).
 - [6] R. Subedi et al., *Science* **320**, 1476 (2008).
 - [7] E. Piasetzky, M. Sargsian, L. Frankfurt, M. Strikman, and J. W. Watson, *Phys. Rev. Lett.* **97**, 162504 (2006).
 - [8] K. Egiyan et al. (CLAS Collaboration), *Phys. Rev. Lett.* **96**, 082501 (2006).
 - [9] N. Fomin et al., *Phys. Rev. Lett.* **108**, 092502 (2012).
 - [10] R. Schiavilla, R. B. Wiringa, S. C. Pieper, and J. Carlson, *Physical Review Letters* **98**, 132501 (2007).
 - [11] I. Korover (2014), 1401.6138.
 - [12] O. Hen et al. (CLAS Collaboration), *Science* (2014), submitted to.
 - [13] R. B. Wiringa, R. Schiavilla, S. C. Pieper, and J. Carlson, *Phys. Rev. C* **89**, 024305 (2014), URL <http://link.aps.org/doi/10.1103/PhysRevC.89.024305>.
 - [14] M. M. Sargsian, *Phys. Rev. C* **89**, 034305 (2014), URL <http://link.aps.org/doi/10.1103/PhysRevC.89.034305>.
 - [15] R. Wiringa, *Private communication*.
 - [16] R. B. Wiringa, V. G. J. Stoks, and R. Schiavilla, *Phys. Rev. C* **51**, 38 (1995), URL <http://link.aps.org/doi/10.1103/PhysRevC.51.38>.
 - [17] S. Veerasamy and W. N. Polyzou, *Phys. Rev. C* **84**, 034003 (2011).
 - [18] S. C. Pieper and R. B. Wiringa, *Annual Review of Nuclear and Particle Science* **51**, 53 (2001).
 - [19] M. Alvioli, C. Ciofi degli Atti, L. P. Kaptari, C. B. Mezzetti, and H. Morita, *Phys. Rev. C* **87**, 034603 (2013), URL <http://link.aps.org/doi/10.1103/PhysRevC.87.034603>.
 - [20] A. Carbone, A. Polls, and A. Rios, *Euro. Phys. Lett.* **97**, 22001 (2012).
 - [21] I. Vidaña, A. Polls, and C. m. c. Providência, *Phys. Rev. C* **84**, 062801 (2011), URL <http://link.aps.org/doi/10.1103/PhysRevC.84.062801>.

- [22] C. Xu, A. Li, and B. Li, J. of Phys: Conference Series **420**, 012190 (2013).
- [23] C. Xu and B. Li (2011), 1104:2075.
- [24] J. M. Lattimer and Y. Lim, Apj **771**, 51 (2013).
- [25] G. A. Fiorentini et al. (MINERvA Collaboration), Phys. Rev. Lett. **111**, 022501 (2013).
- [26] G. A. Fiorentini et al. (MINERvA Collaboration), Phys. Rev. Lett. **111**, 022502 (2013).
- [27] L. Frankfurt and M. Strikman, Phys. Rep. **160**, 235 (1988).
- [28] O. Hen et al., Int. J. Mod. Phys. E **22**, 133017 (2013).
- [29] L. B. Weinstein, E. Piasetzky, D. W. Higinbotham, J. Gomez, O. Hen, and R. Shneor, Phys. Rev. Lett. **106**, 052301 (2011).
- [30] G. P. Zeller et al., **88**, 091802 (2002).
- [31] I. C. Cloet, W. Bentz, and A. W. Thomas, Phys. Rev. Lett. **102**, 252301 (2009).
- [32] *"int workshop, neutrino-nucleus interactions for current and next generation neutrino oscillation experiments (int-13-54w)".*
- [33] S. A. Kulagin and R. Petti, Phys. Rev. C **82**, 054614 (2010).
- [34] O. Hen, E. Piasetzky, and L. B. Weinstein, Phys. Rev. C **85**, 047301 (2012).
- [35] A. Bussiere et al., Nucl. Phys. **A365**, 349 (1981).
- [36] K. Blomqvist et al., Phys. Lett. **B429**, 33 (1998).
- [37] W. U. Boeglin, H. Arenhövel, K. I. Blomqvist, R. Böhm, M. Distler, R. Edelhoff, I. Ewald, R. Florizone, J. Friedrich, R. Geiges, et al., Phys. Rev. C **78**, 054001 (2008).
- [38] P. E. Ulmer, K. A. Aniol, H. Arenhövel, J.-P. Chen, E. Chudakov, D. Crovelli, J. M. Finn, K. G. Fissum, O. Gayou, J. Gomez, et al., Phys. Rev. Lett. **89**, 062301 (2002).
- [39] M. M. Rvachev et al. (Jefferson Lab Hall A Collaboration), Phys. Rev. Lett. **94**, 192302 (2005).
- [40] F. Benmokhtar et al. (Jefferson Lab Hall A Collaboration), Phys. Rev. Lett. **94**, 082305 (2005).
- [41] C. Ciofi degli Atti and L. P. Kaptari, Phys. Rev. Lett. **95**, 052502 (2005), URL <http://link.aps.org/doi/10.1103/PhysRevLett.95.052502>.
- [42] J.-M. Laget, *Photo and electrodisintegration of few body systems revisited* (2003).
- [43] J.-M. Laget, Phys. Lett. **B609**, 49 (2005).
- [44] M. Alvioli, C. C. d. Atti, and L. P. Kaptari, Phys. Rev. C **81**, 021001 (2010), URL <http://link.aps.org/doi/10.1103/PhysRevC.81.021001>.
- [45] A. Johansson, Phys. Rev. **136**, B1030 (1964).

- [46] W. U. Boeglin, L. Coman, P. Ambrozewicz, K. Aniol, J. Arrington, G. Batigne, P. Bosted, A. Camsonne, G. Chang, J. P. Chen, et al. (For the Hall A Collaboration), Phys. Rev. Lett. **107**, 262501 (2011).
- [47] C. Ciofi degli Atti, *Private communication*.
- [48] M. Sargsian, *Private communication*.